Frontiers in Bioscience Landmark

Front. Biosci. (Landmark Ed) **2026**; 31(7): 51761
https://doi.org/10.31083/FBL51761

Original Research

RNA-Binding Protein RBMS3 Inhibits Cervical Cancer Progression by Enhancing HSPA6 mRNA Stability

Huaping Huang[1,2,†], Ping Li[3,†], Lixia Zhu[2], Yawei Wu[2], Qin Liu[2,*], Hong Zhang[1,4,5,*]

[1]The Reproductive Medicine Center, The Second Affiliated Hospital of Soochow University, 215004 Suzhou, Jiangsu, China
[2]Department of Gynecology, The First People's Hospital of Kunshan, 215300 Suzhou, Jiangsu, China
[3]Department of Oncology, The First People's Hospital of Kunshan, 215300 Suzhou, Jiangsu, China
[4]Jiangsu Institute of Clinical Immunology, 215006 Suzhou, Jiangsu, China
[5]Medical Biotechnology Institute, Soochow University, 215031 Suzhou, Jiangsu, China
*Correspondence: liuqinchina@njmu.edu.cn (Qin Liu); szzhanghong@suda.edu.cn (Hong Zhang)
[†]These authors contributed equally.

Academic Editor: Ananda Ayyappan Jaguva Vasudevan
Submitted: 11 March 2026 Revised: 14 May 2026 Accepted: 22 May 2026 Published: 24 July 2026

Abstract

Background: Cervical cancer (CC) is a prevalent malignancy in women. RNA-binding motif single-stranded interacting protein 3 (RBMS3) acts as a tumor suppressor in many cancer types, but its role and underlying regulatory mechanisms in CC remain unclear. **Methods:** The expression levels of RBMS3 and heat shock protein family A member 6 (HSPA6) were evaluated in clinical CC tissues. Gain- and loss-of-function assays, transcriptome sequencing, and rescue experiments were performed in CC cell lines and nude mouse xenograft models. **Results:** RBMS3 expression was notably lower in CC tissues (n = 306) than in normal cervical tissues (n = 22), with reduced levels linked to shorter overall patient survival ($p < 0.05$). Overexpression of RBMS3 reduced cell proliferation, migration, and invasion in vitro, as well as tumor growth *in vivo* ($p < 0.001$). HSPA6 was identified as a key target of RBMS3 and was also downregulated in CC tissues. RBMS3 potentially binds to HSPA6 mRNA and enhances its stability. Knockdown of HSPA6 reversed the tumor-suppressive effects of RBMS3 ($p < 0.001$). **Conclusions:** RBMS3 inhibits CC progression by stabilizing HSPA6 mRNA. The RBMS3–HSPA6 axis may represent a prognostic biomarker and therapeutic target in CC.

Keywords: RNA-binding protein; heat shock protein; post-transcriptional regulation; cervical cancer; tumor suppressor

1. Introduction

Cervical cancer (CC) is a globally prevalent malignant tumor among women and presents a significant public health challenge, particularly in low- and middle-income regions [1]. The development and progression of CC involve complex molecular alterations, including genomic instability, epigenetic silencing, and dysregulated gene expression [2]. Among these regulatory events, RNA-binding proteins (RBPs) have emerged as critical post-transcriptional regulators that modulate mRNA stability, translation, and degradation [3], thereby controlling multiple hallmarks of cancer, including cell proliferation, migration, invasion, and apoptosis [4].

RNA-binding motif single-stranded interacting protein 3 (RBMS3) has been characterized as a vital tumor-suppressive RBP in various human cancer types [5,6,7]. RBMS3 is frequently downregulated in cancers of the breast, lung, esophagus, and colon, and its reduced expression is closely associated with accelerated tumor progression, enhanced metastasis, and poor patient prognosis [5,6,7]. Mechanistically, RBMS3 exerts its anti-tumor functions mainly by stabilizing target mRNAs or by regulating key signaling pathways such as Wnt/β-catenin and liver kinase B1 (LKB1)/AMP-activated protein kinase (AMPK) [6,8]. However, the expression and role of RBMS3 in CC remain poorly understood. Chromosome 3p23-p24, where RBMS3 resides, is frequently deleted in CC, suggesting its potential involvement in cervical carcinogenesis [9]. Nevertheless, whether RBMS3 regulates CC progression and its underlying molecular mechanism remains to be elucidated.

Heat shock protein family A member 6 (HSPA6) is a stress-inducible HSP70 family member that exhibits context-dependent roles in tumorigenesis [10]. It can hinder the growth of colorectal cancers [11], but appears to promote malignancy in other cancer types [12,13]. HSPA6 is hypermethylated in invasive cervical tumors, implying it is potentially involved in malignant progression [14]. Nevertheless, the upstream regulatory mechanism of HSPA6 and its functional relationship with RBMS3 have yet to be explored in CC.

Drawing from prior research, we posited that RBMS3 acts as a tumor suppressor in CC, exerting its influence on HSPA6 through post-transcriptional regulation. The goals of this study included measuring RBMS3 expression in CC tissues, evaluating its association with patient outcome, examining its impact on cancer cell behaviors, identifying

downstream genes, and elucidating the relevant molecular pathways. Our aim was to uncover new biomarkers and treatment avenues for CC.

2. Materials and Methods

2.1 Cell Lines and Experimental Animals

The human CC cell line C-4I was obtained from the American Type Culture Collection in the US, and the SiHa cell line from the National Collection of Authenticated Cell Cultures in Shanghai. Short tandem repeat (STR) profiling was used to confirm cell identity and verify mycoplasma-free status. The cells were grown in Dulbecco's Modified Eagle's Medium (DMEM; HyClone) supplemented with 10% fetal bovine serum (FBS; Gibco) and maintained in a humidified incubator at 37 °C and 5% CO_2.

Female BALB/c nude mice aged 4–6 weeks and weighing 18–22 grams (Specific Pathogen-Free [SPF] grade) were sourced from Shanghai Slack Laboratory Animal Co., Ltd. The mice were kept in an SPF barrier environment at the Experimental Animal Center, The First People's Hospital of Kunshan. At the termination of each experiment, mice were deeply anesthetized with 1.5% isoflurane and then euthanized via cervical dislocation, following national guidelines and an approved ethics protocol.

2.2 Clinical Samples and Tissue Microarray

Between January and December 2024, fresh tumor and corresponding adjacent normal tissues were collected from five CC patients at the First People's Hospital of Kunshan between January 2024 and December 2024. None had undergone radiotherapy, chemotherapy, or targeted therapy prior to surgery, and all patients gave written consent. This study also utilized a commercial CC tissue microarray (Catalog number: HUteS168Su01, Shanghai Xinchao Biotechnology Co., Ltd.) containing 42 normal and 126 cancer tissues.

2.3 TCGA Database Analysis

Transcriptome data and clinical details on CC were sourced from the Cancer Genome Atlas (TCGA) database. This dataset included 22 normal cervical tissue samples, 53 cervical adenocarcinoma samples, and 253 cervical squamous cell carcinoma samples. R software (v4.3.1, R Core Team, Vienna, Austria) and TCGAbiolinks packages were used to normalize the data, extract RBMS3 expression levels, and analyze differences via the Kruskal-Wallis test.

2.4 Construction of Overexpression and Interference Vectors

Overexpression primers and an interference sequence were designed using GenBank data for RBMS3 (NM_001003792.3) and HSPA6 (NM_002155.5). The RBMS3 fragment was inserted into the pLVX-IRES-Puro vector to create an overexpression construct. The HSPA6 shRNA sequence (5′-ACCTCGACTTCTACACGTCCATCACTTCAAGAGAGTGATGGACGTGTAGAAGTCTT-3′) was cloned into the pLKO.1 vector for RNA interference; this shRNA targets the "GACTTCTACACGTCCATCACT" sequence of HSPA6 mRNA. Empty vectors served as controls. All constructs underwent sequencing verification.

2.5 Lentivirus Packaging and Cell Infection

The overexpression or interference vectors were co-transfected with the packaging plasmids psPAX2 and VSV-G (both from Addgene, USA). When C-4I and SiHa cells reached the logarithmic growth phase, they were infected with viral supernatants at an MOI of 10. Then, 8 μg/mL polybrene was added to enhance infection efficiency. After 24 h, the medium was replaced with fresh medium. Selection was begun 48 h later with 2 μg/mL puromycin for two weeks, giving rise to RBMS3 stable overexpressing cell lines (Lv-OE-RBMS3), HSPA6 stable knockdown cell lines (Lv-shHSPA6), and matching control cell lines (Lv-OE-NC, Lv-sh-NC). The success of transfection was verified using real-time qPCR (RT-qPCR) and Western blot, and the transduction efficiency was >80%.

2.6 RT-qPCR

A reverse transcription kit (KR116, Tiangen Biotech Co., Ltd., Beijing, China) was employed to synthesize complementary DNA (cDNA), as recommended by the manufacturer. Glyceraldehyde-3-phosphate dehydrogenase (GAPDH) served as the internal reference for accurate quantification with RT-qPCR. The primer sequences were as follows: RBMS3 forward (5′-TGGACCATCCCATGTCAATGC-3′) and reverse (5′-CCAACGAAAGGTGATTCATCTGC-3′); HSPA6 forward (5′-CATCGCCTATGGGCTGGAC-3′) and reverse (5′-GGAGAGAACCGACACATCGAA-3′); GAPDH forward (5′-GGAGCGAGATCCCTCCAAAAT-3′) and reverse (5′-GGCTGTTGTCATACTTCTCATGG-3′).

2.7 Western Blot Analysis

Cell or tissue samples underwent ice-cold lysis. Protein levels were precisely measured using the bicinchoninic acid assay. Equal protein loads were separated by sodium dodecyl sulfate polyacrylamide gel electrophoresis (SDS-PAGE), and subsequently transferred to polyvinylidene fluoride (PVDF) membranes. Subsequently, membranes were incubated with primary antibodies, including RBMS3 (ab272612), HSPA6 (ab212044), and GAPDH (ab181602) purchased from Abcam (UK). Afterwards, the membranes were incubated with a 1:5000 dilution of HRP-linked secondary antibody at room temperature for one hour to reveal protein bands, followed by quantification of band intensity via ImageJ (v1.54, National Institutes of Health [NIH], Bethesda, MD, USA).

2.8 Immunofluorescence Assay for Protein Localization and Expression

Cells were incubated with primary antibodies against RBMS3 (ab272612) and HSPA6 (ab212044) from Abcam (UK), followed by Alexa Fluor 488- or 594-tagged secondary antibodies. Nuclei were stained with DAPI for 5 minutes at room temperature. Fluorescence images were recorded using an Olympus IX83 microscope and analyzed via ImageJ.

2.9 Immunohistochemical Assay for Tissue Protein Expression

Tissue samples were first blocked with a 5% BSA solution, followed by incubation with primary antibodies against RBMS3 (ab272612), HSPA6 (ab212044), and Ki-67 (ab16667), all purchased from Abcam (UK). Protein expression levels were assessed using the H-Score system, which ranges from 0 to 300 and is calculated as the sum of staining intensity (0–3) multiplied by the proportion of positive cells, times 100.

2.10 CCK-8 Assay

Cells in the logarithmic growth phase were seeded into 96-well plates at a density of 1×10^3 cells per well, with five wells per group. Following incubation periods of 0, 12, 24, 48, 72, and 96 h, 10 µL of CCK-8 reagent (Beyotime, C0037) was added. The absorbance at 450 nm was then recorded, enabling the construction of detailed cell proliferation curves.

2.11 Colony Formation Assay

Cells were evenly distributed in 6-well plates at 1×10^3 cells per well, with three wells per experimental group. They were then cultured under standard conditions for 14 days. Once colonies formed, they were fixed with 4% paraformaldehyde for 15 mins, stained with 0.1% crystal violet for 30 mins, rinsed, and counted (≥50 cells/colony).

2.12 EdU Incorporation Assay

Cells were seeded into 24-well plates at 5×10^4 cells per well and allowed to grow for 24 h. Subsequently, a 50 µM EdU solution was added. After fixing and permeabilizing, the cells were treated with Click-iT reaction mix for 30 minutes. The nuclei were stained briefly with DAPI, and fluorescence microscopy was then used to record images and determine the percentage of EdU-positive cells.

2.13 Scratch Wound Assay

Cells were evenly distributed in 6-well plates and grown until they covered 90% of the surface. A sterile pipette tip was then used to create a straight scratch across the cell layer. After removing detached cells with PBS, serum-free DMEM was added. Images of the scratches were taken at 0 and 24 h using an Olympus CKX41 inverted microscope. Scratch widths were measured with ImageJ, and cell migration distance was determined by subtracting the 24-h width from the 0-h width.

2.14 Transwell Invasion Assay

Matrigel matrix (Corning, USA) was diluted with serum-free DMEM in a 1:8 ratio. Subsequently, 50 µL of this mixture was added to the upper chamber of Transwell inserts (catalog number: 3422, Corning, USA), while 600 µL of DMEM containing 10% FBS was added to the lower chamber. A total of 200,000 cells were then resuspended in serum-free DMEM and placed into the upper chamber. After incubation, any remaining non-invading cells were gently wiped away from the upper side with a cotton swab. Finally, the invading cells were counted in five random fields under an inverted microscope.

2.15 Subcutaneous Xenograft Assay in Nude Mice

Mice were randomly assigned to groups (n = 6 per group). There was no blinding during the experiments or during the evaluation of results. For each group, 200 µL of C-4I cells in the logarithmic growth phase (1×10^7 cells per mL) were injected under the skin on the right dorsal side of a BALB/c nude mouse. Tumor volume was then measured every five days using the formula: tumor volume = length × width^2 / 2. Tumor growth was tracked by plotting curves over time. The mice were sacrificed 30 days after cell injection, and the tumors were removed, weighed, and photographed. A portion of the tumor tissue was fixed with 4% paraformaldehyde for H&E staining and immunohistochemistry, while the remainder was frozen at −80 °C for subsequent experiments.

2.16 Transcriptome Sequencing Analysis

Five biological replicates of C-4I and SiHa cells from both the Lv-OE-RBMS3 and Lv-OE-NC groups underwent transcriptome sequencing (Shanghai OE Biotech Co., Ltd). Total RNA was isolated, and libraries were prepared with the TruSeq Stranded mRNA Library Prep Kit (Cat. No. 20020594, Illumina, Inc., San Diego, CA, USA). Sequencing was carried out on the Illumina NovaSeq 6000 platform via a paired-end 150 bp (PE150) strategy, with a minimum sequencing depth of 6.0 GB (~20–30 million clean reads per sample).

For bioinformatic analysis, raw FastQ data were quality-filtered by fastp (v0.23.0, OpenGene, Shenzhen, China, https://github.com/OpenGene/fastp) to eliminate adapters and low-quality reads. Clean reads were then mapped to the human GRCh38 reference genome using HISAT2 (v2.2.1, Daehwan Kim Lab, UT Southwestern Medical Center, Dallas, TX, USA, https://daehwankimlab.github.io/hisat2/) under default parameters. Gene-level read counts were quantified via featureCounts (v2.0.1, Walter and Eliza Hall Institute of Medical Research, Melbourne, VIC, Australia, http://subread.sourceforge.net/). Differential expression analysis was implemented with the

DESeq2 (v1.34.0, Bioconductor; https://bioconductor.org/packages/DESeq2/) R package. Significantly differentially expressed genes (DEGs) were defined as genes with |logFC| >1 and *p*-values < 0.05. Gene Ontology (GO) functional annotation and Kyoto Encyclopedia of Genes and Genomes (KEGG) pathway enrichment were analyzed using the clusterProfiler (v4.2.0) R package. Overlapping DEGs across cell lines were visualized by Venny 2.1 (BioinfoGP, CNB-CSIC, Madrid, Spain, https://bioinfogp.cnb.csic.es/tools/venny/).

2.17 RNA Immunoprecipitation (RIP) Assay

An RIP kit (catalog number: 17-700, Millipore, USA) was used for this assay. First, 1×10^7 cells from both the Lv-OE-RBMS3 and Lv-OE-NC groups were lysed on ice to maintain intact ribonucleoprotein complexes. After centrifugation of the lysate, the supernatant was divided in two. One half was incubated with 5 µg of biotin-labeled RBMS3 antibody to pull down the RBMS3-RNA complexes, and the other half with 5 µg of IgG antibody as a negative control. Streptavidin magnetic beads (catalog number: P2151, Beyotime, China) were then added to trap the antibody-bound complexes. After washing the beads five times to remove non-specific binding, they were incubated with Proteinase K at 55 °C for 30 minutes to digest proteins and release the RNA. Following the extraction of the RNA, RT-qPCR was performed to assess enrichment with HSPA6 mRNA.

2.18 mRNA Stability Assay

Lv-OE-RBMS3 and Lv-OE-NC cells in the logarithmic growth phase were incubated with 5 µg/mL of actinomycin D (Sigma-Aldrich, USA, cat. no. A9415, Sigma-Aldrich, St. Louis, MO, USA) to halt mRNA synthesis. Samples were then collected at 0, 1, 3, and 6 h, and the total RNA was isolated. RT-qPCR was performed to assess HSPA6 mRNA levels, with residual rates calculated relative to the 0-h baseline.

2.19 Dual-Luciferase Reporter Assay

Dual-luciferase reporter assays were conducted to assess the potential association between RBMS3 and HSPA6 mRNA. Specifically, the full-length HSPA6 mRNA sequence (including a 1932-nucleotide CDS and a 304-nucleotide 3′UTR region) was inserted into the reporter constructs. Within the context of this full-length sequence, vectors containing either the wild-type binding motif AATTTATT (HSPA6-WT) or the mutated sequence GGCCCGCC (HSPA6-Mutant) were generated to evaluate binding specificity. This motif corresponds to nucleotides 195–202 of the HSPA6 3′UTR (numbered from the start of the 3′UTR). These vectors were co-transfected into C-4I and SiHa cells alongside either pLVX-RBMS3 or pLVX-NC vectors. After 48 h, luciferase activities were measured, with Renilla activity serving as an internal control for the calculation of relative activity.

2.20 Statistical Analysis

Each experiment was performed independently and at least in triplicate. SPSS 26.0 (v26.0, IBM Corporation, Armonk, NY, USA) and GraphPad Prism 9.0 (v9.0, GraphPad Software, LLC, San Diego, CA, USA) were used for statistical analysis. Data are shown as the mean ± standard deviation (SD). Before running any tests, the data was examined for normal distribution and whether the variances were equal. The two-tailed Student's *t*-test was used to compare two groups. For more than two groups, one-way analysis of variance (ANOVA) with Tukey's post hoc test was used. Overall survival analysis was performed using the clinical follow-up data linked to the 126 CC samples from the commercial tissue microarray cohort. For this analysis, the median H-Score obtained from immunohistochemical staining was established as the predefined cutoff value, stratifying patients into "High RBMS3" and "Low RBMS3" expression groups. The Kaplan-Meier method was utilized to generate survival curves, and the log-rank test was applied to evaluate the statistical significance of differences in survival outcomes. For the results presented in each figure, the statistical test used is explicitly stated in the corresponding figure legend. Results were considered to be statistically significant when the *p*-value was < 0.05.

3. Results

3.1 RBMS3 is Downregulated in Cervical Cancer Tissues and Correlates With Poor Patient Prognosis

Analysis of the TCGA database revealed that RBMS3 mRNA levels were significantly lower in both cervical adenocarcinoma (n = 53) and cervical squamous cell carcinoma (n = 253) compared to normal cervical tissue (n = 22) ($p < 0.001$, Fig. 1A). RBMS3 mRNA (Fig. 1B) and protein (Fig. 1C) levels were consistently lower in five CC tissues than in paired adjacent normal tissues ($p < 0.05$). Immunohistochemical analysis of tissue arrays confirmed that RBMS3 protein expression was lower in CC tissues compared to normal tissues (Fig. 1D). This was also apparent from the lower H-Score in the cancer samples compared to normal tissue ($p < 0.001$, Fig. 1E). Patients with low RBMS3 expression in the tissue arrays showed worse survival compared to those with higher levels (HR = 1.990, 95% CI: 1.034–3.828, $p = 0.039$, Fig. 1F), indicating that RBMS3 could be a useful prognostic marker in CC.

3.2 Construction and Validation of RBMS3-Overexpressing Cervical Cancer Cell Lines

Lentiviral vectors were used to create RBMS3-overexpressing cell lines (Lv-OE-RBMS3) and control lines (Lv-OE-NC) in both C-4I and SiHa cells. RT-qPCR showed that RBMS3 mRNA levels were markedly higher in Lv-OE-RBMS3 cells compared to controls ($p < 0.001$, **Supplementary Fig. 1A**). Western blot analysis confirmed that RBMS3 protein levels were also much higher in the overexpression group ($p < 0.001$, **Supplementary**

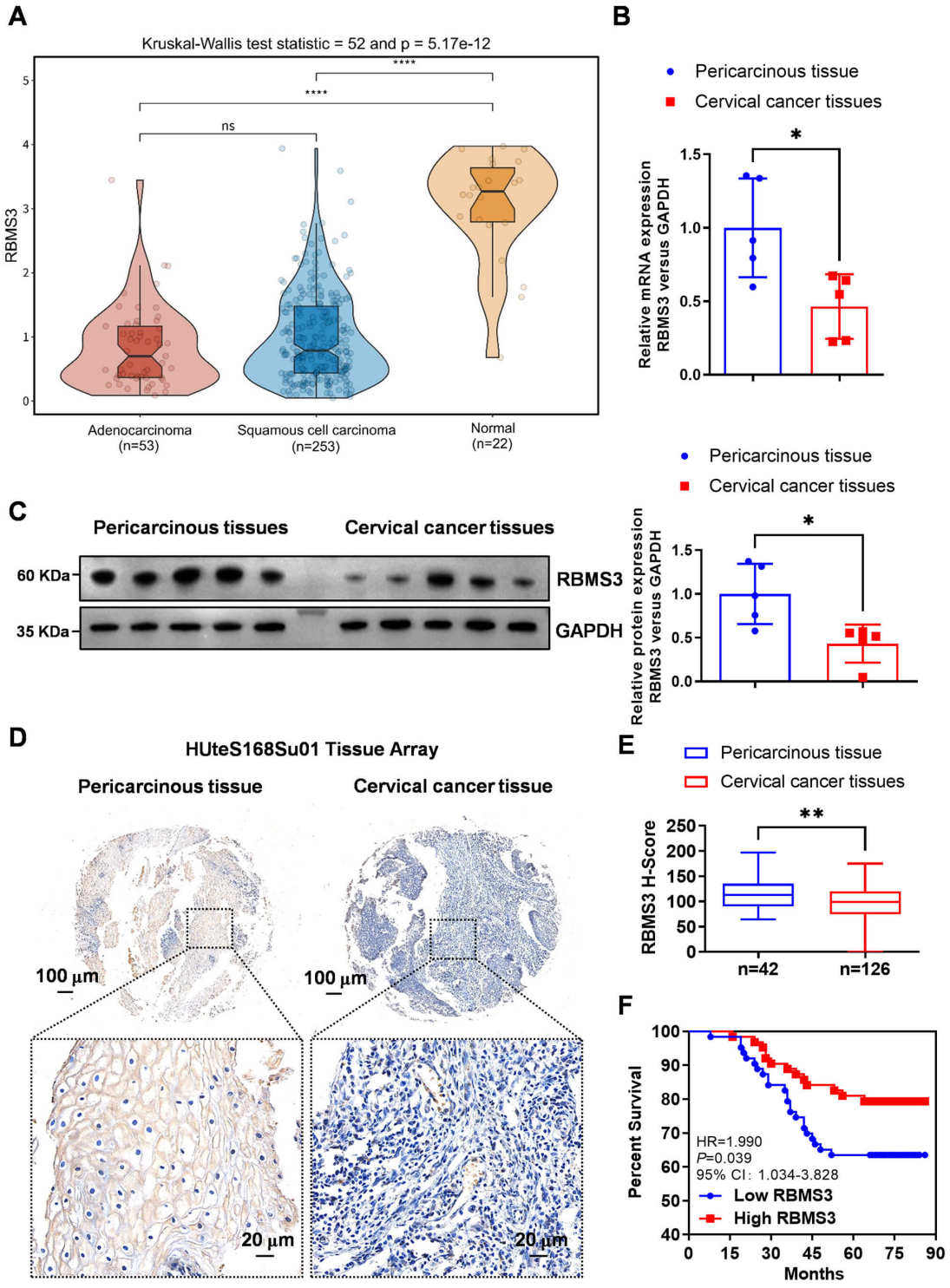

Fig. 1. RBMS3 is downregulated in CC tissues. (A) RBMS3 mRNA levels in CC tissues and normal cervical tissues from the TCGA database. (B,C) RT-qPCR and Western blot analyses showing RBMS3 expression in five matched pairs of fresh CC and normal tissues. (D) Representative immunohistochemistry images of RBMS3 protein expression across a 168-sample CC tissue microarray. (E) H-Score results of RBMS3 expression from the tissue microarray. (F) Survival analysis for RBMS3 expression in CC patients from the tissue microarray. Data show the mean ± SD. A two-tailed Student's *t*-test or log-rank test was used for statistical analysis. ns, not significant, $^{*}p < 0.05$, $^{**}p < 0.01$, $^{****}p < 0.0001$. Scale bars: 100 μm for low-magnification overview images in (D), 20 μm for high-magnification enlarged fields in (D). RBMS3, RNA-binding motif single-stranded interacting protein 3; CC, cervical cancer; TCGA, the Cancer Genome Atlas; RT-qPCR, real-time qPCR.

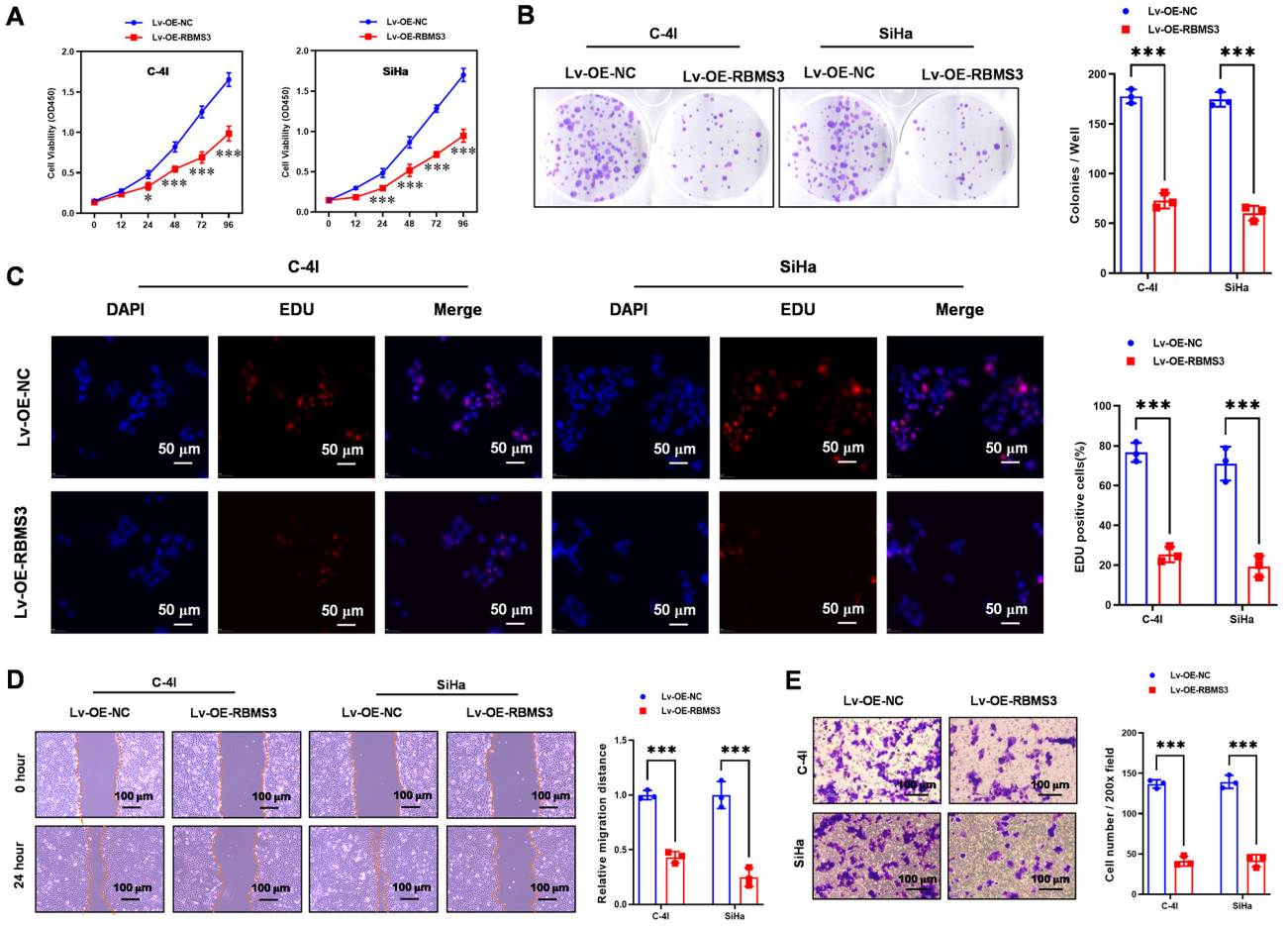

Fig. 2. RBMS3 overexpression inhibits the proliferation, migration, and invasion of CC cells. (A–C) The CCK-8 assay, colony formation assay, and EdU incorporation assay were used to evaluate the effect of RBMS3 overexpression on CC cell proliferation. (D) Scratch wound assay showing the effect of RBMS3 overexpression on CC cell migration. (E) Transwell invasion assay showing the effect of RBMS3 overexpression on CC cell invasion ability. Cells were divided into two groups: Lv-OE-NC (empty vector control) and Lv-OE-RBMS3 (RBMS3 overexpression). Data show the mean ± SD (n = 3). A two-tailed Student's *t*-test was used for the statistical analysis. $^{*}p < 0.05$, $^{***}p < 0.001$. Scale bars: 50 μm for (C), 100 μm for (D,E).

Fig. 1B). Immunofluorescence revealed that RBMS3 was mostly located in the cytoplasm, and that Lv-OE-RBMS3 cells showed much stronger fluorescence than the controls (**Supplementary Fig. 1C**).

3.3 RBMS3 Overexpression Inhibits the Proliferation, Migration, and Invasion of Cervical Cancer Cells

The CCK-8 assay was used to examine the growth of CC cells. In both C-4I and SiHa cells, the absorbance values for the Lv-OE-RBMS3 group were significantly lower at 24, 48, 72, and 96 h compared to the Lv-OE-NC controls ($p < 0.05$, Fig. 2A). Additionally, Lv-OE-RBMS3 cells formed significantly fewer colonies than the controls ($p < 0.001$, Fig. 2B), and fewer EdU-positive cells were seen in the Lv-OE-RBMS3 group than in the controls ($p < 0.001$, Fig. 2C). The scratch wound assay revealed that C-4I and SiHa cells in the Lv-OE-RBMS3 group did not migrate as far after 24 h compared to the control group ($p < 0.001$, Fig. 2D). Similarly, the transwell invasion assay showed less invasion by Lv-OE-RBMS3 cells compared to the control ($p < 0.001$, Fig. 2E). These results imply that overexpression of RBMS3 suppresses DNA synthesis, proliferation, migration, and invasion in CC cells.

3.4 RBMS3 Overexpression Inhibits the Tumorigenicity of Cervical Cancer Cells in Nude Mice

To study the *in vivo* effects of RBMS3 on CC growth, C-4I cells from both the Lv-OE-RBMS3 and Lv-OE-NC groups were injected under the skin of BALB/c nude mice to establish subcutaneous xenograft models. The resulting tumors in the Lv-OE-RBMS3 group were significantly smaller and lighter than those in the control group (Fig. 3A). Tumors in the Lv-OE-RBMS3 group grew more slowly over time than the controls ($p < 0.001$, Fig. 3B), and their weight was significantly lighter than that of tumors from the control group ($p < 0.001$, Fig. 3C). H&E staining

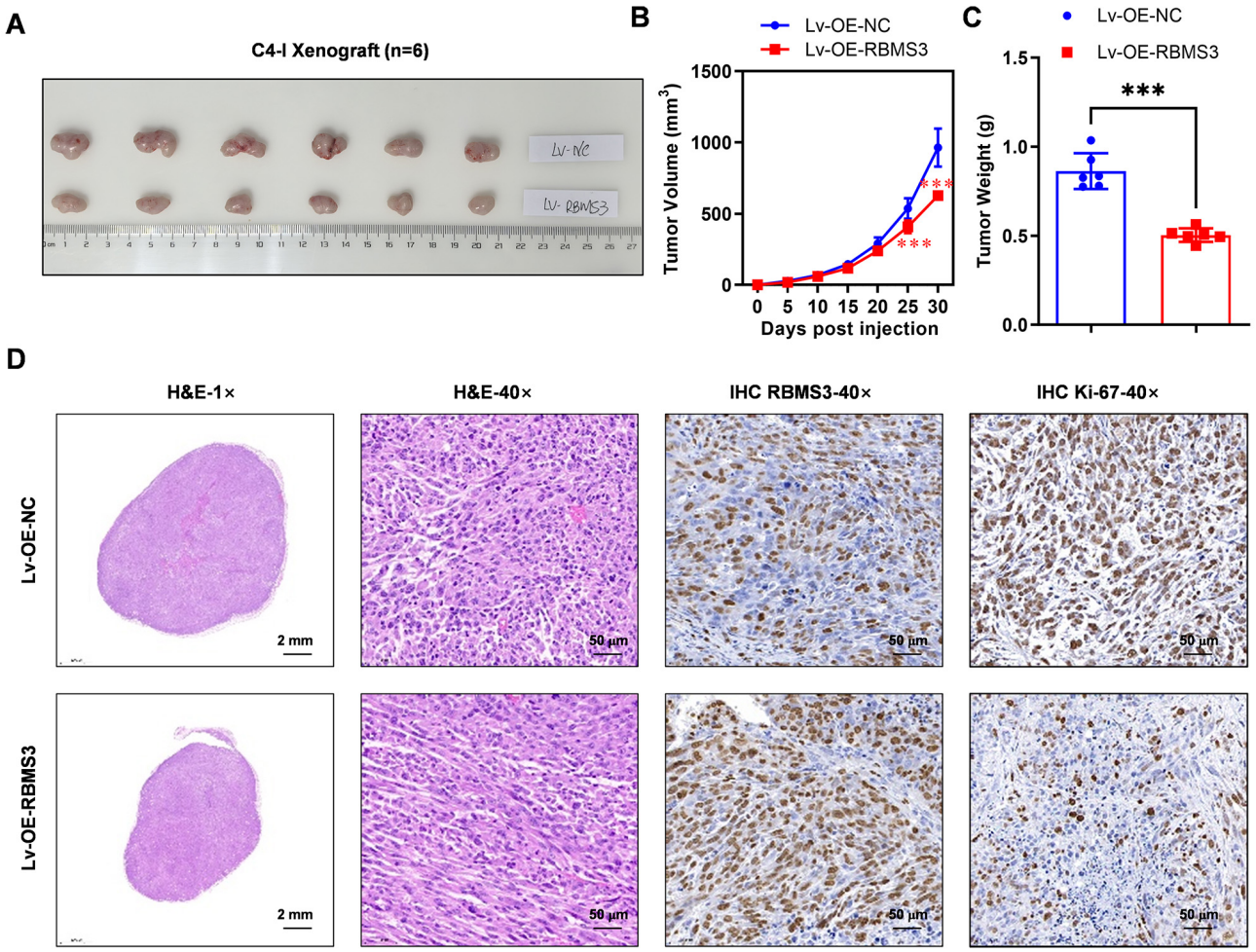

Fig. 3. RBMS3 overexpression suppresses tumor growth *in vivo*. (A) Images of xenograft tumors from nude mice injected with RBMS3-overexpressing or control cells. (B) Graph showing tumor volume at the indicated time points. (C) Tumor weight at the end of the experiment. (D) Immunohistochemical staining of RBMS3 and Ki-67 in xenograft tumor tissues. Cells were divided into two groups: Lv-OE-NC (empty vector control) and Lv-OE-RBMS3 (RBMS3 overexpression). Data show the mean ± SD (n = 6). Student's *t*-test was used for statistical analysis. $^{***}p < 0.001$ vs. control group. Scale bars: 2 mm for low-magnification H&E images in (D), 50 μm for high-magnification H&E and immunohistochemistry images in (D).

of tumor tissues from the Lv-OE-RBMS3 group revealed a notable decline in tumor cell proliferation (Fig. 3D).

3.5 Transcriptome Sequencing Identifies Downstream Target Genes of RBMS3

To investigate the role of RBMS3 in CC, transcriptome sequencing was performed on C-4I and SiHa cells from both the Lv-OE-RBMS3 and Lv-OE-NC groups. RBMS3 overexpression was associated with many changes in gene expression. In SiHa cells, 2044 genes were upregulated, and 2590 were downregulated, while in C-4I cells, 2623 genes were upregulated and 2945 were downregulated ($|\log FC| > 1$, $p < 0.05$). Heatmaps displaying the top 10 significantly upregulated and downregulated DEGs in SiHa and C-4I cells are presented in Fig. 4A,B, respectively. KEGG pathway enrichment analysis revealed the upregulated DEGs were mainly enriched in inflammatory and immune-related signaling pathways, along with tumor-associated signaling cascades and cellular stress/response processes (Fig. 4C,D).

Venn diagram analysis showed that 955 of the DEGs were common to both cell lines (Fig. 4E). Of these, the top 10 upregulated genes for each cell line are shown in Fig. 4F. Since HSPA6 was the most consistent and significantly upregulated gene in both CC cell lines (Fig. 4F), subsequent investigations focused on this gene. In clinical samples, both HSPA6 mRNA (Fig. 4G) and protein (Fig. 4H) levels were much lower in the cancer tissue compared to normal tissue ($p < 0.01$). Moreover, both HSPA6 mRNA (Fig. 5A) and protein (Fig. 5B) levels were significantly higher in the Lv-OE-RBMS3 group compared to the Lv-OE-NC group ($p < 0.01$). Immunofluorescence confirmed that HSPA6 was mostly located in the cytoplasm, and its fluorescence was much stronger in the Lv-OE-RBMS3 group than in the con-

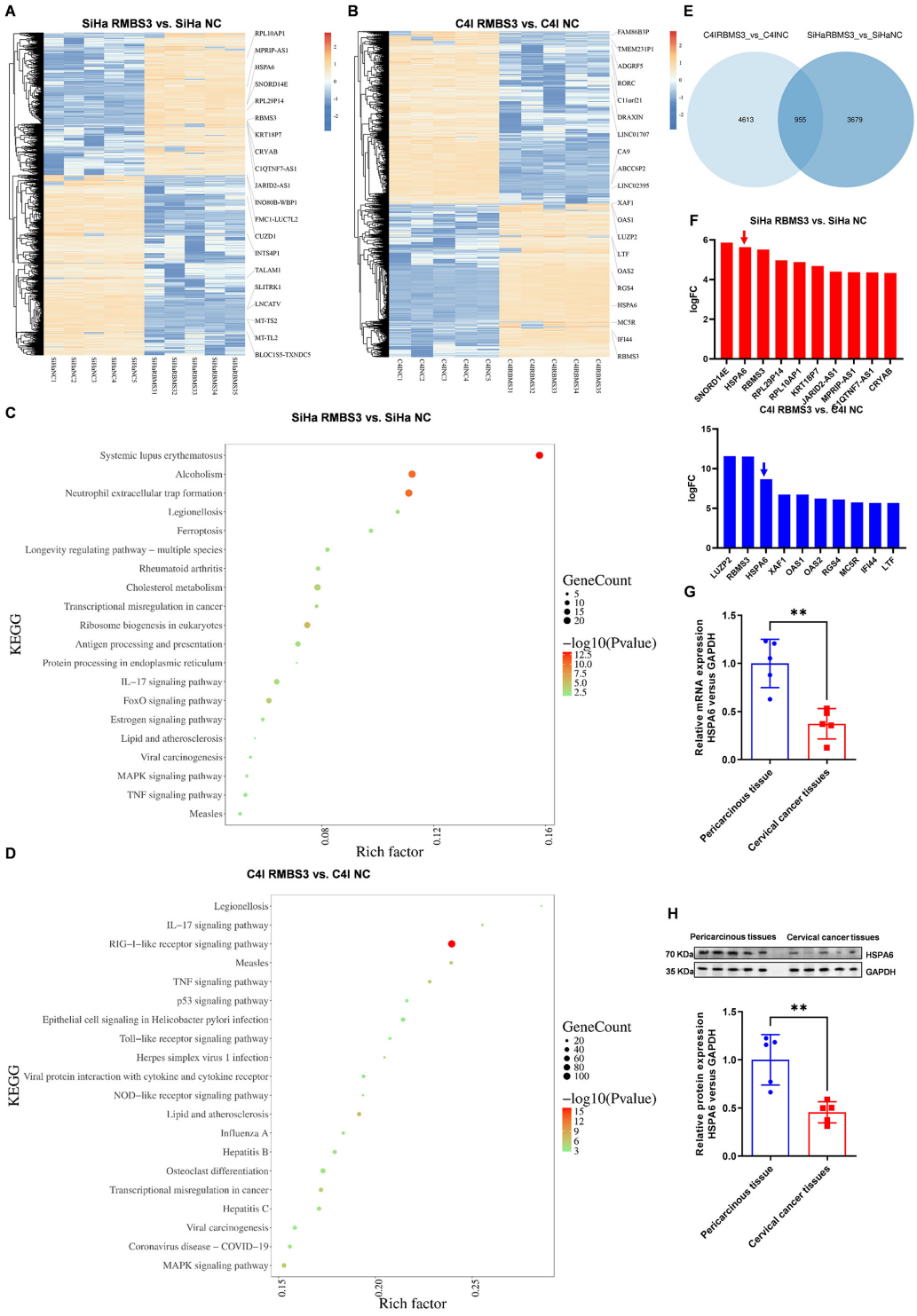

Fig. 4. HSPA6 is identified as a key downstream target of RBMS3. (A,B) Heatmaps of the top 10 significantly upregulated and downregulated differentially expressed genes (DEGs) in SiHa and C-4I cells after RBMS3 overexpression (|logFC| >1, $p < 0.05$). (C,D) KEGG pathway analysis highlights the main pathways activated in CC cells with RBMS3 overexpression. (E) Venn analysis showing 955 DEGs upon RBMS3 overexpression that were found in both cell lines. (F) Top 10 upregulated genes in both cell lines after RBMS3 overexpression. (G,H) RT-qPCR and Western blot analyses showing the differential expression of HSPA6 between five fresh CC samples and their matching normal tissues. Data show the mean ± SD (n = 5). A two-tailed Student's *t*-test was used for statistical analysis. $^{**}p < 0.01$.

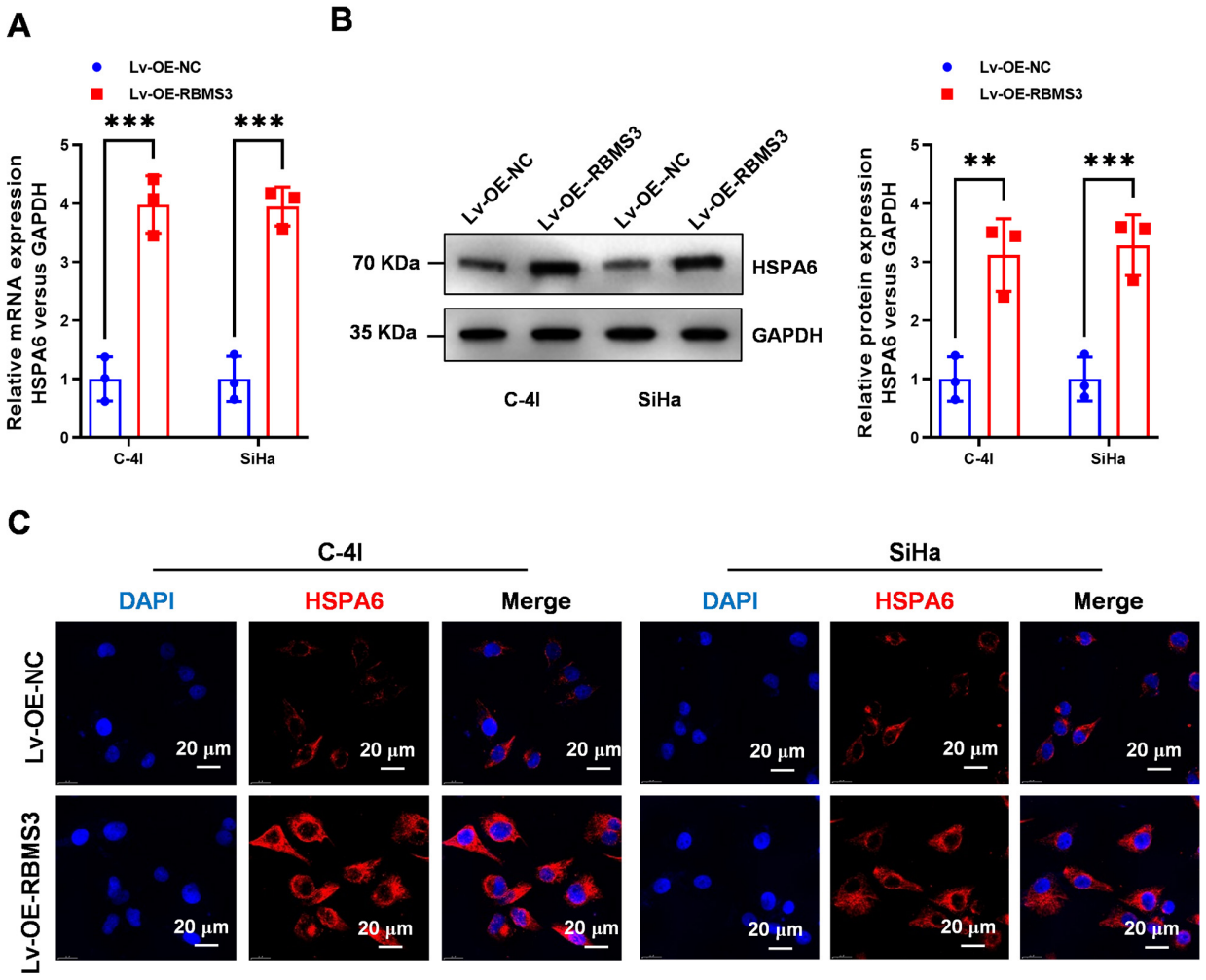

Fig. 5. RBMS3 overexpression upregulates HSPA6 expression. (A,B) RT-qPCR and Western blot analyses of HSPA6 expression in RBMS3-overexpressing cell lines. (C) Immunofluorescence validation of HSPA6 expression in RBMS3-overexpressing cell lines. Cells were divided into two groups: Lv-OE-NC (empty vector control) and Lv-OE-RBMS3 (RBMS3 overexpression). Data show the mean ± SD (n = 3). A two-tailed Student's *t*-test was used for statistical analysis. $^{**}p < 0.01$, $^{***}p < 0.001$. Scale bar: 20 μm for (C).

trol group (Fig. 5C). Collectively, these results suggest that HSPA6 is a key downstream target of RBMS3.

3.6 RBMS3 Enhances HSPA6 mRNA Stability

To investigate the role of HSPA6 in CC, lentiviral transduction was first used to construct stable cell lines that overexpress HSPA6 (Lv-OE-HSPA6). HSPA6 mRNA and protein levels were markedly higher in Lv-OE-HSPA6 cells compared to the controls ($p < 0.001$, **Supplementary Fig. 2A,B**). Functional assays revealed that HSPA6 overexpression was associated with slower growth of CC cells. Moreover, the CCK-8 assays showed less absorbance at 48, 72, and 96 h ($p < 0.05$, **Supplementary Fig. 2C**), indicating fewer cells. Colony formation assays confirmed that fewer colonies formed when HSPA6 was overexpressed ($p < 0.001$, **Supplementary Fig. 2D**). Moreover, the scratch wound assay showed less migration of Lv-OE-HSPA6 cells after 24 h ($p < 0.01$, **Supplementary Fig. 2E**). These findings indicate that overexpression of HSPA6 slows the growth and migration of CC cells.

To investigate how RBMS3 regulates HSPA6, a RIP assay was performed to determine whether RBMS3 binds to HSPA6 mRNA. Significantly more HSPA6 mRNA was pulled down by the RBMS3 antibody than the IgG control ($p < 0.05$, Fig. 6A). Next, the HSPA6 mRNA level was evaluated following the blocking of new mRNA synthesis with actinomycin D. Overexpression of RBMS3 (Lv-OE-RBMS3) sustained higher residual levels of HSPA6 mRNA compared with the control group (Lv-OE-NC), indicating that RBMS3 stabilizes HSPA6 mRNA ($p < 0.05$, Fig. 6B).

We further constructed two dual-luciferase reporter vectors with full-length HSPA6 mRNA: one containing a normal HSPA6 binding site (HSPA6-WT) and the other containing a mutated version (HSPA6-Mutant). These vectors were co-transfected with an RBMS3 overexpression

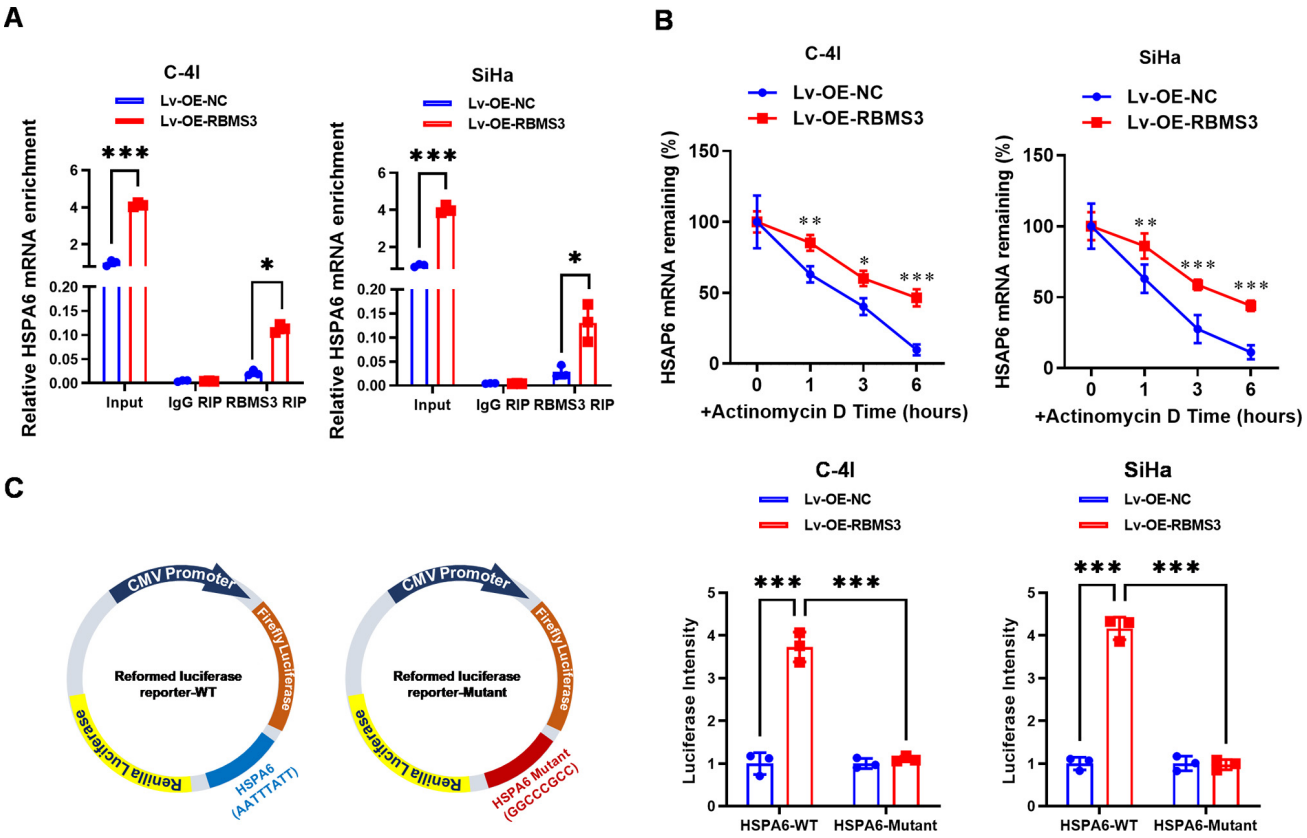

Fig. 6. RBMS3 potentially binds to HSPA6 mRNA and enhances its stability. (A) RNA immunoprecipitation (RIP) assay showing the enrichment of HSPA6 mRNA by RBMS3. (B) RT-qPCR evaluation of the residual HSPA6 mRNA level in CC cells following the inhibition of mRNA synthesis with actinomycin D. (C) Dual-luciferase reporter assay confirms the interaction between RBMS3 and HSPA6 mRNA. Cells were divided into two groups: Lv-OE-NC (empty vector control) and Lv-OE-RBMS3 (RBMS3 overexpression). Data show the mean ± SD (n = 3). A two-tailed Student's *t*-test was used for statistical analysis. $^{*}p < 0.05$, $^{**}p < 0.01$, $^{***}p < 0.001$ vs. control group.

plasmid into C-4I and SiHa cells. Cells with both the RBMS3 plasmid and the HSPA6-WT vector showed a large increase in luciferase activity compared to the empty vector control ($p < 0.001$), whereas luciferase activity was barely altered with the mutant vector (Fig. 6C). Therefore, RBMS3 appears to enhance the stability of HSPA6 mRNA.

3.7 Construction and Validation of HSPA6-Knockdown Cell Lines

Cell lines that concurrently overexpress RBMS3 and exhibit HSPA6 knockdown (Lv-OE-RBMS3 + Lv-shHSPA6) were used to investigate how HSPA6 interacts with RBMS3 to affect CC progression. Three control groups were also used: Lv-OE-NC + Lv-sh-NC, Lv-OE-RBMS3 + Lv-sh-NC, and Lv-OE-NC + Lv-shHSPA6. The levels of HSPA6 mRNA and protein were significantly lower in the Lv-OE-RBMS3 + Lv-shHSPA6 group compared to the Lv-OE-RBMS3 + Lv-sh-NC group ($p < 0.001$), whereas the mRNA and protein levels of RBMS3 were unchanged (**Supplementary Fig. 3A,B**). These results indicate successful construction of the HSPA6-knockdown model.

3.8 HSPA6 Knockdown Reverses the Inhibitory Effects of RBMS3 Overexpression on the Proliferation, Migration, and Invasion of Cervical Cancer Cells

The CCK-8 assay demonstrated that cells in the Lv-OE-RBMS3 + Lv-shHSPA6 group displayed a higher proliferation rate relative to the Lv-OE-RBMS3 + Lv-sh-NC group ($p < 0.001$, Fig. 7A). Moreover, the colony formation assay showed the Lv-OE-RBMS3 + Lv-shHSPA6 group produced significantly more colonies ($p < 0.001$, Fig. 7B). This group also exhibited a much higher proportion of EdU-positive cells compared to the control ($p < 0.001$, Fig. 7C).

The scratch wound assay showed that cells from the Lv-OE-RBMS3 + Lv-shHSPA6 group migrated much farther after 24 h than those in the Lv-OE-RBMS3 + Lv-sh-NC group ($p < 0.001$, Fig. 8A). Similarly, the transwell invasion assay revealed that cells from the Lv-OE-RBMS3 + Lv-shHSPA6 group were significantly more invasive compared to control cells ($p < 0.001$, Fig. 8B). Thus, knockdown of HSPA6 attenuates the effect of RBMS3 overexpression and restores the ability of CC cells to migrate and invade.

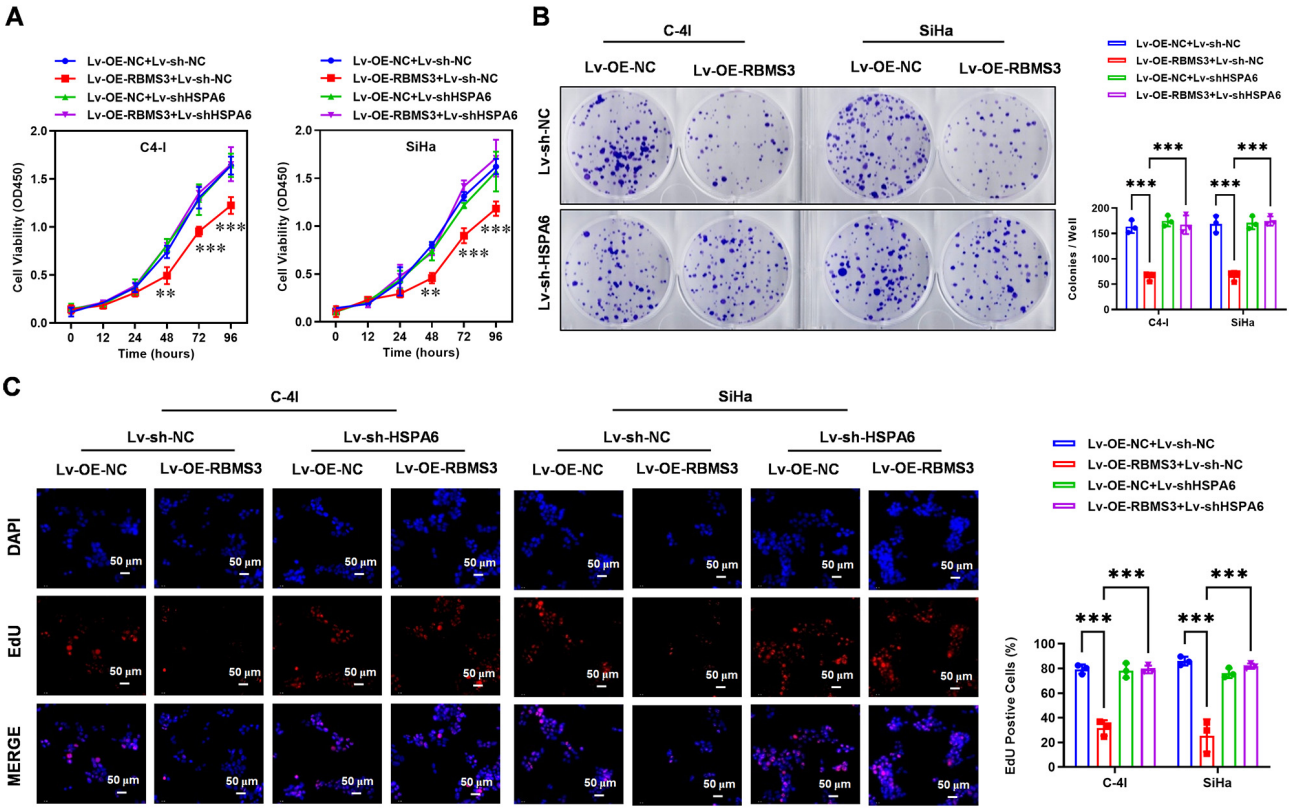

Fig. 7. HSPA6 knockdown reverses the inhibitory effect of RBMS3 on cell proliferation. (A–C) CCK-8 assay, colony formation assay, and EdU incorporation assay show the effects of concurrent RBMS3 overexpression and HSPA6 knockdown on cell proliferation. Cells were divided into four groups: Lv-OE-NC + Lv-sh-NC (empty vector + shRNA negative control), Lv-OE-RBMS3 + Lv-sh-NC (RBMS3 overexpression + shRNA negative control), Lv-OE-NC + Lv-sh-HSPA6 (empty vector + HSPA6 knockdown), and Lv-OE-RBMS3 + Lv-sh-HSPA6 (RBMS3 overexpression + HSPA6 knockdown). Data shown are the mean ± SD (n = 3). One-way analysis of variance (ANOVA) was used for statistical analysis. $^{**}p < 0.01$, $^{***}p < 0.001$. Scale bar: 50 μm for (C).

3.9 HSPA6 Knockdown Reverses the Inhibitory Effect of RBMS3 Overexpression on the Tumorigenicity of Cervical Cancer Cells In Vivo

C-4I cells from four groups (Lv-OE-NC + Lv-sh-NC, Lv-OE-RBMS3 + Lv-sh-NC, Lv-OE-NC + Lv-shHSPA6, and Lv-OE-RBMS3 + Lv-shHSPA6) were injected under the skin of BALB/c nude mice to create subcutaneous xenograft models. Tumors derived from the Lv-OE-RBMS3 + Lv-shHSPA6 group were larger in size (Fig. 9A) and displayed an accelerated growth rate (Fig. 9B) relative to the Lv-OE-RBMS3 + Lv-sh-NC group ($p < 0.001$). Moreover, the tumors were significantly heavier at the end of the study compared to the Lv-OE-RBMS3 + Lv-sh-NC group ($p < 0.001$, Fig. 9C).

H&E staining revealed that tumor cells from the Lv-OE-RBMS3 + Lv-shHSPA6 group displayed enhanced proliferative activity relative to the Lv-OE-RBMS3 + Lv-sh-NC group (Fig. 9D). Immunohistochemistry revealed less expression of HSPA6 protein in the Lv-OE-RBMS3 + Lv-shHSPA6 tumors, but a higher frequency of Ki-67 positive cells compared to the control group (Fig. 9E). Therefore, knockdown of HSPA6 expression attenuates the growth-suppressing effect of RBMS3 overexpression on CC cells *in vivo*.

4. Discussion

The present study found lower expression of RBMS3 in CC tissues compared to normal tissue, with the down-regulation linked to worse clinical outcomes. This result concurs with previous reports in several other cancer types that RBMS3 acts as a tumor suppressor [5,6,7]. RBMS3 is an RNA-binding protein, and earlier studies showed that it can slow cancer growth by controlling the stability of certain mRNAs and affecting downstream signaling [5]. In the current investigation, increased expression of RBMS3 slowed the growth, migration, and invasive capacity of CC cells *in vitro*. Additionally, overexpression of RBMS3 in CC cells injected into mice slowed the growth of xenograft tumors. Therefore, similar to other cancer types, the present results suggest that RBMS3 also hinders the growth of CC.

Transcriptome profiling combined with mechanistic validation identified HSPA6 as a key downstream target of RBMS3. HSPA6 was consistently upregulated upon RBMS3 overexpression. Further assays showed that

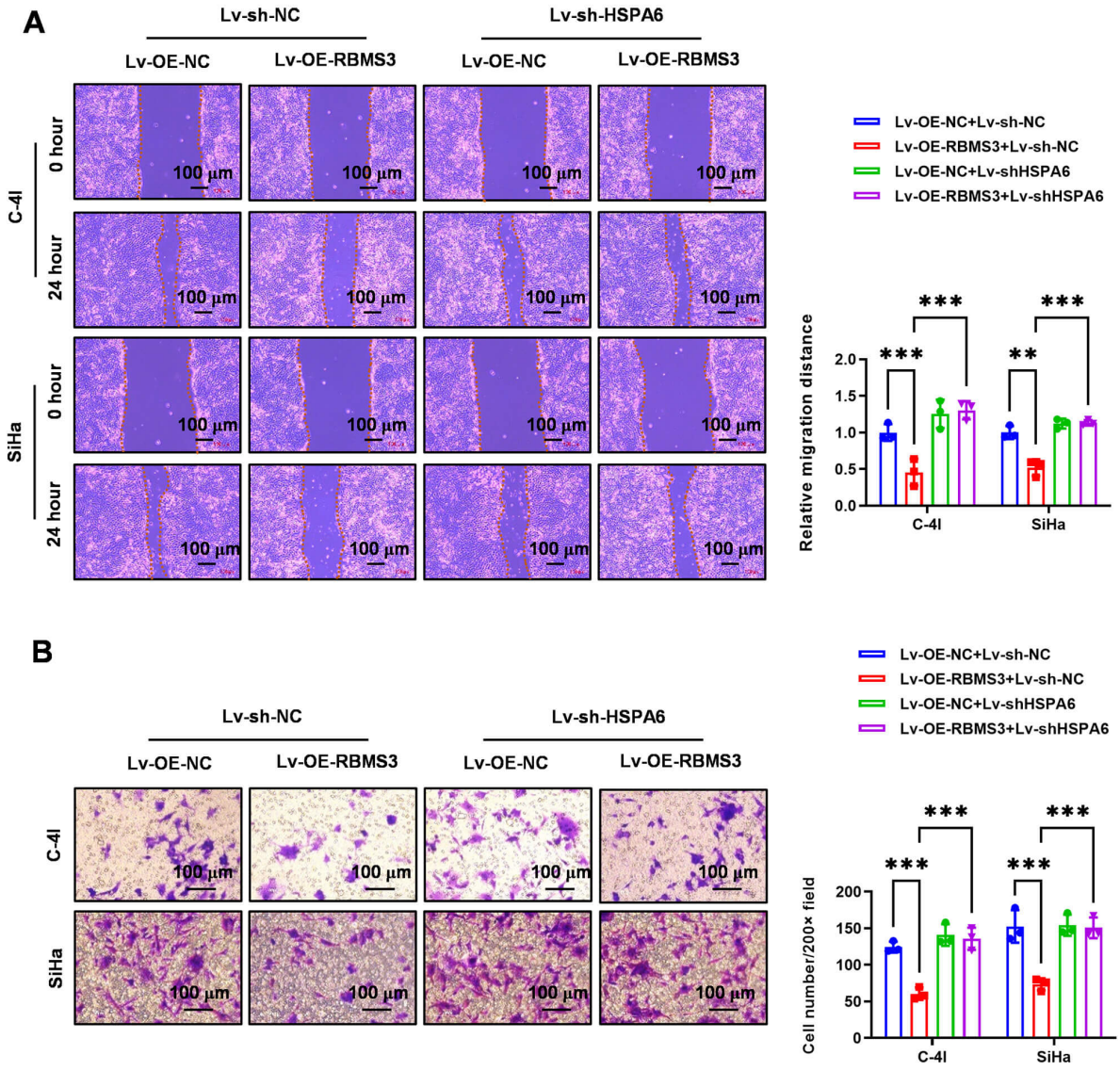

Fig. 8. HSPA6 knockdown reverses the inhibitory effect of RBMS3 on cell migration and invasion. (A) Scratch wound assay showing the effects of concurrent RBMS3 overexpression and HSPA6 knockdown on cell migration. (B) Transwell invasion assay showing the effects of concurrent RBMS3 overexpression and HSPA6 knockdown on cell invasion ability. Cells were divided into four groups: Lv-OE-NC + Lv-sh-NC (empty vector + shRNA negative control), Lv-OE-RBMS3 + Lv-sh-NC (RBMS3 overexpression + shRNA negative control), Lv-OE-NC + Lv-sh-HSPA6 (empty vector + HSPA6 knockdown), and Lv-OE-RBMS3 + Lv-sh-HSPA6 (RBMS3 overexpression + HSPA6 knockdown). Data show the mean ± SD (n = 3). One-way ANOVA was used for statistical analysis. $^{**}p < 0.01$, $^{***}p < 0.001$. Scale bars: 100 μm for (A,B).

RBMS3 potentially binds to HSPA6 mRNA and enhances its stability, thereby increasing HSPA6 expression at both the mRNA and protein levels. Rescue experiments revealed that HSPA6 knockdown reversed the inhibitory effects induced by RBMS3 overexpression, indicating that HSPA6 is a functional mediator of RBMS3 in CC. Together, these results establish the RBMS3–HSPA6 axis as a novel post-transcriptional regulatory pathway governing the progression of CC.

HSPA6 is a stress-inducible member of the HSP70 chaperone family and plays varied roles in different cancer types [10]. Although it can be triggered by cellular stress [10], our study found notably lower basal HSPA6 levels in CC tissues than in adjacent normal tissues. These observations suggest that the physiological basal expression of HSPA6 may be relevant to cervical carcinogenesis and stress responses. Dysregulation of basal HSPA6 levels could contribute to malignancy independently of acute stress, although this requires further experimental validation.

The RBMS3–HSPA6 axis holds promise as a useful biomarker for CC and as a possible target for novel

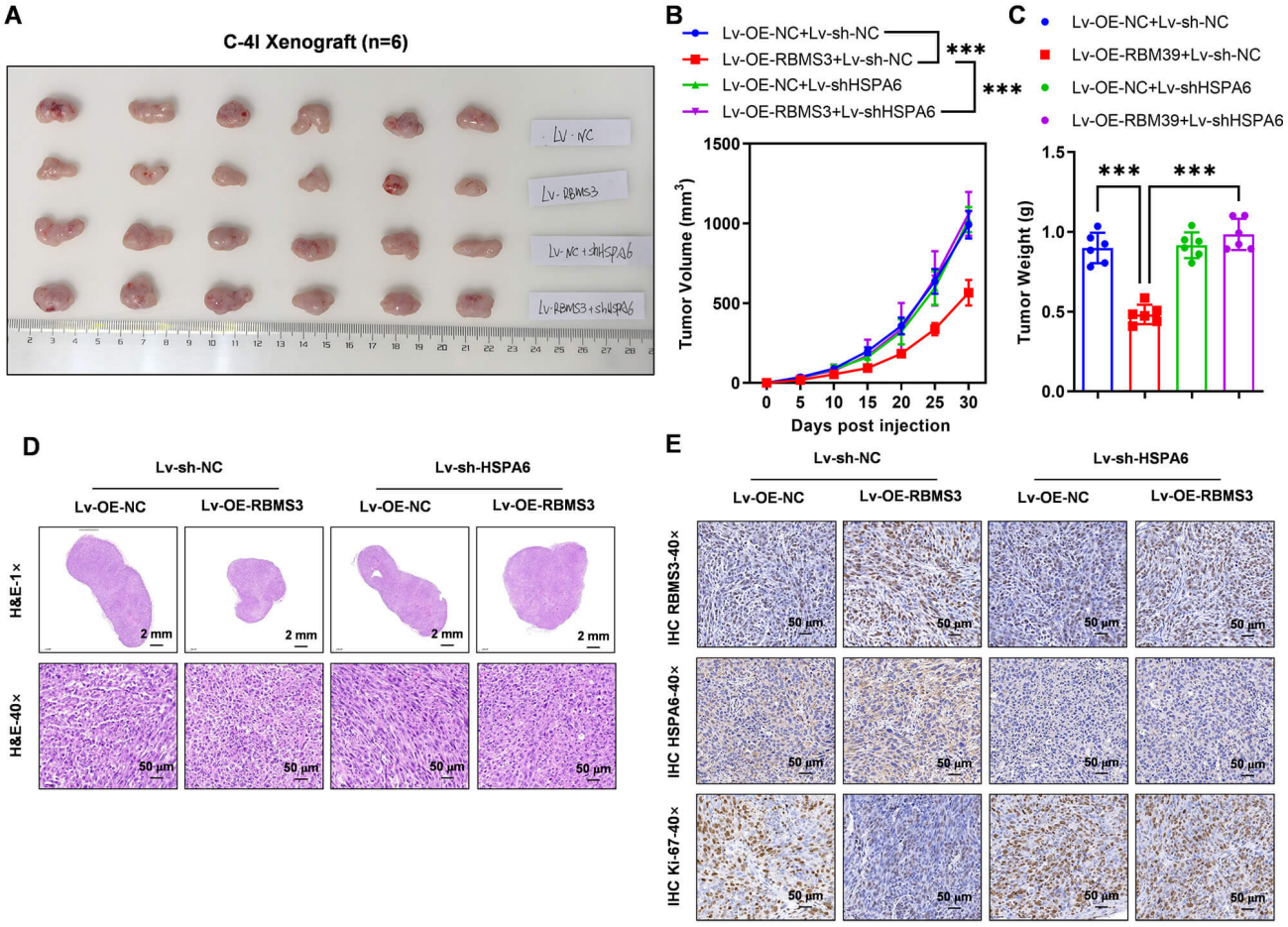

Fig. 9. HSPA6 knockdown reverses the inhibitory effect of RBMS3 on tumor growth. (A) Photographs of xenograft tumors from different treatment groups. (B) Graph of tumor volume measured at the indicated time points. (C) Tumor weight at the end of the experiment. (D,E) H&E staining and immunohistochemistry validate the expression of RBMS3, HSPA6, and Ki-67 in xenograft tumor tissues. Mice were randomly assigned to four groups according to the transfected C-4I cells they received: Lv-OE-NC + Lv-sh-NC (empty vector + shRNA negative control), Lv-OE-RBMS3 + Lv-sh-NC (RBMS3 overexpression + shRNA negative control), Lv-OE-NC + Lv-sh-HSPA6 (empty vector + HSPA6 knockdown), and Lv-OE-RBMS3 + Lv-sh-HSPA6 (RBMS3 overexpression + HSPA6 knockdown). Data show the mean ± SD (n = 6). One-way ANOVA was used for statistical analysis. $^{***}p < 0.001$. Scale bars: 2 mm for low-magnification H&E images in (D), 50 μm for high-magnification H&E images in (D) and all immunohistochemistry images in (E).

treatments. Restoration of RBMS3 expression may represent a potential strategy to upregulate HSPA6 and constrain CC progression. However, potential therapeutic applications, including those involving epigenetic modulation [15,16], require further experimental validation before clinical translation can be envisaged.

While the current study showed that RBMS3 overexpression slows the growth, migration, and invasion of CC cells, further work is needed to determine whether this involves epithelial-mesenchymal transition and apoptosis. This should provide a clearer picture of the role of the RBMS3–HSPA6 axis in CC cells.

5. Limitations

Several limitations of this study should be acknowledged. First, since the clinical sample size was small and samples were derived from only one center, the prognostic findings may not apply to a wider group. Second, the HPV oncoproteins E6/E7 are central to cervical carcinogenesis [1,17], and hence future studies should investigate the potential interplay between E6/E7 and the RBMS3–HSPA6 axis. Comparison of the RBMS3–HSPA6 axis across different malignancies will also help to clarify the cancer specificity and upstream regulatory mechanisms of this axis. Third, the upstream regulatory mechanism of RBMS3 and its precise binding motif on HSPA6 mRNA requires further clarification. In addition, the antitumor effect of the RBMS3–HSPA6 axis alone was moderate, and its impact on the tumor immune microenvironment was not explored.

6. Conclusions

CC tissues express low levels of RBMS3 compared to normal tissue. Moreover, low tumor expression of RBMS3 is associated with poor patient prognosis. The overexpression of RBMS3 in CC cells reduces their *in vitro*, growth, migration, and invasion, and leads to smaller tumors in animal xenograft models. Mechanistically, RBMS3 potentially binds to HSPA6 mRNA and maintains its stability, thereby increasing the cellular HSPA6 level. Furthermore, knockdown of HSPA6 reverses the tumor-suppressive effects induced by RBMS3 overexpression. Collectively, these results indicate that RBMS3 inhibits the progression of CC by enhancing the stability of HSPA6 mRNA. The RBMS3–HSPA6 axis may therefore serve as a biomarker of prognosis and as a novel target for therapy.

Availability of Data and Materials

The original data supporting the key findings of this study will be made available to qualified researchers upon reasonable request. Corresponding de-identified clinical sample data and related experimental records will be shared only after obtaining approval from the aforementioned ethics committee and signing a data use agreement to ensure compliance with patient privacy regulations. Raw transcriptome sequencing data have been deposited in the Gene Expression Omnibus (GEO) database under the accession number GSE328374.

Author Contributions

HH: Writing - original draft; Methodology; Data curation; Formal analysis. PL: Validation; Software; Data curation; Visualization; Writing-review & editing. LZ: Investigation; Writing-review & editing; Project administration; Resources. YW: Software; Methodology; Project administration. QL: Conceptualization; Funding acquisition; Writing-review & editing; Methodology. HZ: Conceptualization; Funding acquisition; Methodology; Writing-review & editing. All authors contributed to editorial changes in the manuscript. All authors read and approved the final manuscript. All authors have participated sufficiently in the work and agreed to be accountable for all aspects of the work.

Ethics Approval and Consent to Participate

The study was carried out in accordance with the guidelines of the Declaration of Helsinki. The research protocol for clinical sample collection was approved by the Ethics Committee of the First People's Hospital of Kunshan (Approval No.: IEC-SOP-007-A07-V5.0). Written informed consent was obtained from all patients prior to the collection of fresh cervical cancer tissues and corresponding adjacent normal tissues. The animal experimental protocol was approved by the Animal Ethics Committee of the First People's Hospital of Kunshan (Approval No.: KSPH-IACUC-20250008). All animal experimental procedures were conducted in accordance with the principles of the 3Rs (Replacement, Reduction, and Refinement), and the study was reported following the ARRIVE guidelines for animal research. All animal procedures adhered to the National Guidelines for the Care and Use of Laboratory Animals (China).

Acknowledgment

Not applicable.

Funding

National Natural Science Foundation of China (82571922, 82504077) and Natural Science Project of Jiangsu Province (BK20241791).

Conflicts of Interest

The authors declare no conflicts of interest.

Declaration of AI and AI-Assisted Technologies in the Writing Process

During the preparation of this manuscript, the authors utilized ChatGPT (developed by OpenAI) to assist with spelling correction and grammar improvement. Following the use of this tool, the authors conducted a thorough review and revision of the content to guarantee its accuracy and clarity. The authors bear full responsibility for the content of this publication and clearly confirm that the scientific interpretation, data analysis, and conclusions were independently formulated and validated by the authors. The application of AI was restricted to linguistic polishing and did not affect the scientific outcomes or integrity of the study.

Supplementary Material

Supplementary material associated with this article can be found, in the online version, at https://doi.org/10.31083/FBL51761.

References

[1] Bhatla N, Aoki D, Sharma DN, Sankaranarayanan R. Cancer of the cervix uteri: 2025 update. International Journal of Gynaecology and Obstetrics: the Official Organ of the International Federation of Gynaecology and Obstetrics. 2025; 171: 87–108. https://doi.org/10.1002/ijgo.70277

[2] Fay J, Kelehan P, Lambkin H, Schwartz S. Increased expression of cellular RNA-binding proteins in HPV-induced neoplasia and cervical cancer. Journal of Medical Virology. 2009; 81: 897–907. https://doi.org/10.1002/jmv.21406

[3] Glisovic T, Bachorik JL, Yong J, Dreyfuss G. RNA-binding proteins and post-transcriptional gene regulation. FEBS Letters. 2008; 582: 1977–1986. https://doi.org/10.1016/j.febslet.2008.03.004

[4] Qin H, Ni H, Liu Y, Yuan Y, Xi T, Li X, et al. RNA-binding proteins in tumor progression. Journal of Hematology & Oncology. 2020; 13: 90. https://doi.org/10.1186/s13045-020-00927-w

[5] Xin Z, Huang H, Shao Y. Function and Mechanism of the RNA-binding Protein RBMS3 in Malignant Tumours. Cell Biochem-

istry and Biophysics. 2025; 83: 4313–4322. https://doi.org/10.1007/s12013-025-01859-3

[6] Lv SL, Zhou X, Li YJ, Luo LY, Huang DQ. RBMS3, a downstream target of AMPK, Exerts Inhibitory Effects on Invasion and Metastasis of Lung Cancer. Journal of Cancer. 2023; 14: 2784–2797. https://doi.org/10.7150/jca.86572

[7] Li Y, Chen L, Nie CJ, Zeng TT, Liu H, Mao X, et al. Downregulation of RBMS3 is associated with poor prognosis in esophageal squamous cell carcinoma. Cancer Research. 2011; 71: 6106–6115. https://doi.org/10.1158/0008-5472.CAN-10-4291

[8] Li Y, Wang S, Li G, Gao C, Cui Z, Cong M, et al. The RNA-binding protein RBMS3 inhibits the progression of colon cancer by regulating the stability of LIMS1 mRNA. Cancer Medicine. 2024; 13: e7129. https://doi.org/10.1002/cam4.7129

[9] Herzog CR, Crist KA, Sabourin CL, Kelloff GJ, Boone CW, Stoner GD, et al. Chromosome 3p tumor-suppressor gene alterations in cervical carcinomas. Molecular Carcinogenesis. 2001; 30: 159–168. https://doi.org/10.1002/mc.1024

[10] Song B, Shen S, Fu S, Fu J. HSPA6 and its role in cancers and other diseases. Molecular Biology Reports. 2022; 49: 10565–10577. https://doi.org/10.1007/s11033-022-07641-5

[11] Fan Q, Liu B. Identification of the anticancer effects of a novel proteasome inhibitor, ixazomib, on colorectal cancer using a combined method of microarray and bioinformatics analysis. OncoTargets and Therapy. 2017; 10: 3591–3606. https://doi.org/10.2147/OTT.S139686

[12] Yang Z, Zhuang L, Szatmary P, Wen L, Sun H, Lu Y, et al. Upregulation of heat shock proteins (HSPA12A, HSP90B1, HSPA4, HSPA5 and HSPA6) in tumour tissues is associated with poor outcomes from HBV-related early-stage hepatocellular carcinoma. International Journal of Medical Sciences. 2015; 12: 256–263. https://doi.org/10.7150/ijms.10735

[13] Guo X, Wang Y, Zhang H, Qin C, Cheng A, Liu J, et al. Identification of the Prognostic Value of Immune-Related Genes in Esophageal Cancer. Frontiers in Genetics. 2020; 11: 989. https://doi.org/10.3389/fgene.2020.00989

[14] Su PH, Hsu YW, Huang RL, Weng YC, Wang HC, Chen YC, et al. Methylomics of nitroxidative stress on precancerous cells reveals DNA methylation alteration at the transition from *in situ* to invasive cervical cancer. Oncotarget. 2017; 8: 65281–65291. https://doi.org/10.18632/oncotarget.18370

[15] Duncan RM, Reyes L, Moats K, Robinson RM, Murphy SA, Kaur B, et al. ATF3 Coordinates Antitumor Synergy between Epigenetic Drugs and Protein Disulfide Isomerase Inhibitors. Cancer Research. 2020; 80: 3279–3291. https://doi.org/10.1158/0008-5472.CAN-19-4046

[16] Zhao Y, Wang Y, Zhang X, Han S, Yang B. Metformin-induced RBMS3 expression enhances ferroptosis and suppresses ovarian cancer progression. Reproductive Biology. 2025; 25: 100968. https://doi.org/10.1016/j.repbio.2024.100968

[17] Wilailak S, Kengsakul M, Kehoe S. Strategic approaches for global cervical cancer elimination: An update review and call for national action. International Journal of Gynaecology and Obstetrics: the Official Organ of the International Federation of Gynaecology and Obstetrics. 2025; 171: 120–128. https://doi.org/10.1002/ijgo.70276